INTERNATIONAL JOURNAL FOR NUMERICAL METHODS IN FLUIDS, VOL. 19, 889–903 (1994)

A NUMERICAL METHOD FOR ACCELERATING THE RATE OF CONVERGENCE OF THE SIMPLE-LIKE ALGORITHM FOR FLOW THROUGH A THIN FILTER

X. WEN AND D. B. INGHAM

Department of Applied Mathematical Studies, University of Leeds, Leeds LS2 9JT, U.K.

SUMMARY

The control volume, finite difference method and the k–ε turbulence model are employed in a numerical simulation of the turbulent fluid flow both outside and inside a blunt cylindrical sampler which houses a paper filter in its chamber. The presence of a paper filter, which has a very large resistance, results in a large pressure drop across the filter and this causes difficulties in making the SIMPLE or the SIMPLEC scheme converge. In order to improve the rate of convergence of the SIMPLE-like algorithm when the resistance of the filter is very large, an average pressure correction formula is proposed. Based on global mass conservation, a line average pressure correction for the paper filter is derived using a modified Darcy law for a porous medium. A combination of this formula and the SIMPLE-like algorithm can rapidly build up the pressure drop across the filter and hence dramatically improve the rate of convergence of the iterative scheme. Comparisons of the convergence histories and the numerical results for the fluid flow when using SIMPLE and SIMPLEC with the average pressure correction method show that the average pressure correction method for dealing with the paper filter significantly accelerates the rate of convergence of the iterative scheme.

KEY WORDS SIMPLE-like algorithm Average pressure correction Paper filter Turbulent flow Sampler

1. INTRODUCTION

Dust samplers are widely used in the workplace and ambient atmospheres so that portions of dust-laden air may be aspirated and collected on a paper filter which is housed in the chamber of the sampler. This sample is then assessed and the concentration of airborne dust determined. The chamber of the sampler is designed so as to control the shape and strength of the recirculating fluid flow in the chamber. This is necessary because we wish to avoid the particles impacting on the wall of the chamber of the sampler and to control the particle distribution on the filter so that an efficient operation of the filter and an accurate particle measurement may be made. Therefore the simulation of the fluid flow in the chamber of a sampler is very important in the design of samplers.

The paper filters used in the chamber of samplers are usually of very small thickness, typically of the order of 10^{-4} m, with a penetration coefficient of about 10^{9}. Therefore the pressure drop that the fluid undergoes on passing through the filter is very large and is greater than elsewhere in the fluid field by several orders of magnitude. As discussed by Wen and Ingham,[1] a rapid variation in the pressure usually results in a very slow rate of convergence of the SIMPLE-like algorithms as developed by Patankar[2] and Van Doormaal and Raithby.[3] This is because the global mass conservation is obtained by the local mass conservation through the elliptical pressure correction equation and this equation is not very sensitive to rapid changes in the fluid velocity which are caused by rapid changes in the geometry of the problem. Based on the global mass conservation principle, Wen and Ingham[1] integrated the

CCC 0271–2091/94/220889–15

Received December 1993
Revised April 1994

momentum equation for an approximate one-dimensional flow and derived a line average pressure correction which is a result of the average velocity correction. The formula obtained by Wen and Ingham[1] can significantly accelerate the rate of convergence of the iterative procedure when rapid pressure changes are caused by rapid changes in the geometry of the solution domain. Hence a similar procedure has been developed for dealing with the large pressure drops which are produced by the resistance of a paper filter. We employ the k–ε turbulence model and the control volume, finite difference method in order to simulate the turbulent flow both inside and outside the sampler in which a paper filter is housed. A numerical model of the paper filter is developed by use of a staggered grid and an average pressure correction is derived based on the global mass conservation and a modified Darcy law for the fluid flow through a porous medium. It is found that when the resistance of the filter is very large, the average pressure correction procedure developed in this paper can significantly accelerate the rate of convergence of the iterative scheme.

2. GOVERNING EQUATIONS

In general, the dust-laden fluid flows are two phase flows and turbulent convection, turbulent diffusion and the inertial force caused by the dust particles affect the motion of the fluid. The dust particles do not follow the motion of the air owing to their inertia, and the distortion of the fluid flow produces a non-uniform distribution of dust particles, i.e. the concentration of the particles is not constant in the fluid flow. The interaction between the fluid and dust particles and the variation in the concentration of the dust particles become more important as the size of the dust particles increases. However, in this paper we have neglected this interaction between the fluid and dust particles and assumed that the existence of the particles does not change the turbulent structure of the fluid flow and that the density of the (two-phase) fluid flow is constant. In practical aerosol sampling this will be a good approximation because the particles are normally less than 50 μm in diameter and in very low concentrations. Because the collection of particles on the filter will change the resistance of the filter, the fluid flow will be time-dependent. However, as a first approximation in our understanding of the basic fluid and particle mechanics of this system we have ignored this time-dependent change in the resistance of the filter. Further, it is possible that some of the particles which are initially deposited on the filter may be re-entrained into the fluid flow. In order to fully investigate this phenomenon, the nature of the filter and particles needs to be specified, and to reduce the complexity of the problem, it is assumed that once a particle has hit the filter it sticks to it. The use of all of these approximations allows us to employ a standard turbulent flow model for the simulation of the fluid flow.

In order to illustrate the numerical technique used for dealing with the fluid flow through a thin filter with a large penetration efficiency, we consider the fluid flow past an axisymmetric disc of radius R and thickness d which faces the wind, and the air is sampled through a circular central orifice of radius r_0. Behind the disc is a cylindrical sampling chamber of radius r_1 and length l and an exit pipe of radius r_2. The axes of the disc, the cylindrical chamber and the outlet pipe are all aligned. The dust-laden air enters the chamber through the orifice of the sampler, passes through a paper filter on which the particles are collected and is then pumped out through the exit pipe. Cylindrical co-ordinates (see Figure 1) are used in which r is the co-ordinate in the radial direction and z is aligned with the axis of symmetry of the sampler and is measured positively in the opposite direction to the direction of the freestream.

The turbulent air flow through filters is governed by the modified Darcy law[1] which can be expressed as

$$\frac{1}{\rho}\nabla P = -\frac{1}{\rho}(\alpha \mathbf{V} + \beta|\mathbf{V}|\mathbf{V}), \tag{1}$$

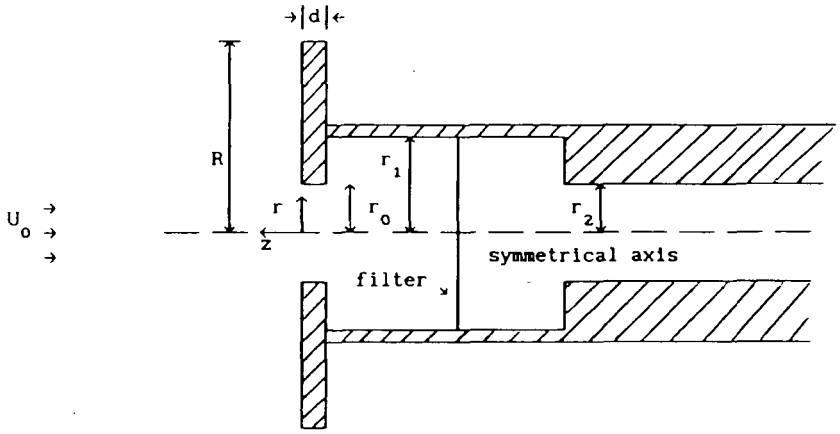

Figure 1. Mathematical model of blunt sampler

where ∇P is the pressure gradient across the filter, V is the fluid velocity vector through the filter and α and β are permeability coefficients which depend on the physical properties of the porous medium and the fluid. Therefore the momentum equation for the turbulent fluid flow in the presence of a filter is given by

$$\mathbf{V}\cdot\nabla\mathbf{V} = -\nabla p + \nabla\cdot(\nu_e\nabla\mathbf{V}) - \frac{1}{\rho}(\alpha\mathbf{V} + \beta|\mathbf{V}|\mathbf{V}), \tag{2}$$

where $p = P/\rho$ and α and β are identically zero in all of the computational domain except on the filter. For an incompressible turbulent fluid we also have the continuity equation

$$\nabla\cdot\mathbf{V} = 0, \tag{3}$$

where $V = ue_r + we_z$ is the turbulent averaged velocity vector, u and w are the turbulent averaged velocity components in the radial and axial directions respectively, ρ is the density of the fluid and υ_e is the effective kinematic viscosity of the fluid, consisting of the sum of the laminar kinematic viscosity υ and the turbulent kinematic viscosity υ_t, i.e. $\upsilon + \upsilon_t$. It should be noted that we have assumed that the fluid is incompressible because the fluid velocities are not very large. However, because of the rapid changes in pressure that occur in these problems, the density will vary, but under practical aerosol sampling conditions this variation in the density of the fluid is not significant.

A standard k–ε turbulence model, as developed by Lauder and Spalding,[4] is employed and the governing equations are as follows. The *turbulent kinetic energy equation* is

$$(\mathbf{V}\cdot\nabla)k = \nabla\cdot\left[\left(\nu + \frac{\nu_t}{\sigma_k}\right)\nabla k\right] + \phi - \varepsilon, \tag{4}$$

the *turbulent energy dissipation equation* is

$$(\mathbf{V}\cdot\nabla)\varepsilon = \nabla\cdot\left[\left(\nu + \frac{\nu_t}{\sigma_\varepsilon}\right)\nabla\varepsilon\right] + C_1\frac{\varepsilon}{k}\phi - C_2\frac{\varepsilon^2}{k} \tag{5}$$

and the *turbulent viscosity* is given by

$$\nu_t = C_\mu\frac{k^2}{\varepsilon}, \tag{6}$$

where k is the turbulent kinetic energy, ε is the turbulent dissipation and ϕ is the generation of turbulent energy which is caused by turbulent stresses. The coefficients which occur in equations (4)–(6) are those used in the standard k–ε equations:[4]

$$C_\mu = 0{\cdot}09, \quad \sigma_k = 1{\cdot}0, \quad \sigma_\epsilon = 1{\cdot}3_{,1} = 1{\cdot}44, \quad C_2 = 1{\cdot}92. \tag{7}$$

These values are based on extensive examination of free flows but can also be used for wall flows, although the constants need to be changed in order to accommodate for effects such as curvature and low Reynolds number. In fact, we found that the numerically predicted values of k and ε are in good agreement with the experimental values obtained by Vincent *et al.*[5]

3. BOUNDARY CONDITIONS

Equations (2)–(5) now have to be solved subject to the appropriate boundary conditions. Since the sampler is axisymmetric, we need only consider the solution in the semi-infinite domain $r > 0$, $-\infty < z < \infty$ (see Figure 2). However, in the numerical calculations we have to approximate the location of the boundary conditions as $r \to \infty$, $-\infty < z < \infty$ to be at a finite radius, i.e. on AB, and as $z \to \pm\infty$ at finite distances, i.e. on AA′ and BB′. Equations (2)–(5) now have to be solved subject to the following boundary conditions.

On the upstream boundary AA′ the fluid velocity takes the constant value U_0 in the negative z-direction. For the freestream turbulence we use the experimental data obtained by Vincent *et al.*,[5] who used an adjustable system of square-mesh, biplanar-lattice-type grids. They give empirical expressions for the freestream turbulent intensity I and the turbulent length scale L as

$$I = 1.59\left(\frac{x}{b}\right)^{-0.7}, \tag{8}$$

$$\frac{L}{b} = 0.02\left(\frac{x}{b}\right)^{1.03}, \tag{9}$$

where b and x are the width of the bars in the grid system and the distance downstream from the grid system respectively.

On the freestream boundary AB

$$\frac{\partial u}{\partial r} = \frac{\partial w}{\partial r} = \frac{\partial k}{\partial r} = \frac{\partial \varepsilon}{\partial r} = 0 \tag{10}$$

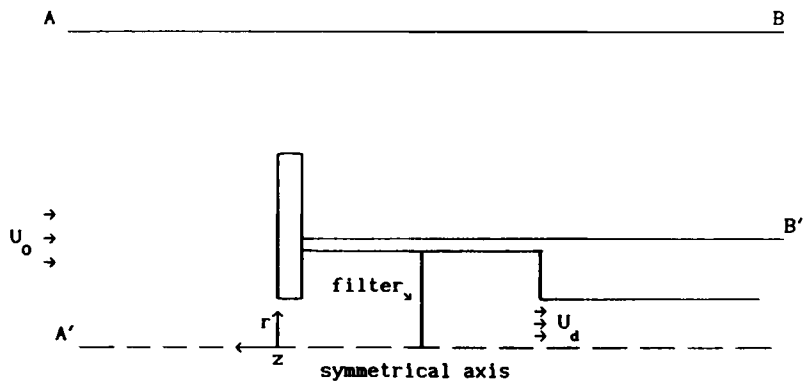

Figure 2. Computational domain

On the downstream boundary BB'

$$\frac{\partial u}{\partial z} = \frac{\partial w}{\partial z} = \frac{\partial k}{\partial z} = \frac{\partial \varepsilon}{\partial z} = 0. \tag{11}$$

On the axis of symmetry

$$u = 0, \qquad \frac{\partial w}{\partial r} = \frac{\partial k}{\partial r} = \frac{\partial \varepsilon}{\partial r} = 0. \tag{12}$$

At the entrance of the exit pipe of the sampler it is assumed that there is a uniform velocity U_{ds} which corresponds to a sampling flow rate Q and $\partial k/\partial z = \partial \varepsilon/\partial z = 0$.

Near the walls of the sampler the wall function method[4] is used to bridge the fully turbulent region and the flow in the vicinity of the wall. When the grid node P which is nearest to the wall of the sampler is located at a distance y from the wall, the value of the quantity y^+ at the point P is defined as

$$y^+ = \left(\frac{C_\mu^{1/4} k^{1/2} y}{\nu}\right)_{\text{p}}. \tag{13}$$

For the momentum equations the wall shear stress τ_{w} is calculated using the linear or the logarithmic law of the wall, i.e.

$$\tau_{\text{w}} = \left(\nu \frac{U}{y}\right)_{\text{p}} \quad \text{for } y^+ \leq 11, \tag{14}$$

$$\tau_{\text{w}} = \left(\frac{\rho \kappa C_\mu^{1/4} k^{1/2} U}{\ln(Ey^+)}\right)_{\text{p}} \quad \text{for } y^+ \geq 11, \tag{15}$$

where the Karman constant $\kappa = 0.4$, for a smooth wall $E = 9{\cdot}0$ and U is the component of the fluid velocity parallel to the wall.

In the k-equation (4) the source term $S_k = \phi - \varepsilon$ at the point P nearest to the wall is modified by use of the wall function. The generation term ϕ is calculated by use of the wall shear stress expression (14) or (15), whilst the dissipation term ε is calculated from

$$\varepsilon_{\text{p}} = \left(\frac{C_\mu^{3/4} k^{3/2} y^+}{y}\right)_{\text{p}} \quad \text{for } y^+ \leq 11, \tag{16}$$

$$\varepsilon_{\text{p}} = \left(\frac{C_\mu^{3/4} k^{3/2} \ln(Ey^+)}{\kappa y}\right)_{\text{p}} \quad \text{for } y^+ \geq 11. \tag{17}$$

In the ε-equation (5) the value of ε at the point P is calculated from

$$\varepsilon_{\text{p}} = \left(\frac{C_\mu^{3/4} k^{3/2}}{\kappa y}\right)_{\text{p}}. \tag{18}$$

4. MATHEMATICAL MODEL OF THE FILTER AND THE NUMERICAL METHOD

The control volume, finite difference method is used to discretize the governing equations (2)–(5) on a non-uniform staggered grid. Because the thickness of the filter is much smaller than that of the control volume, the axial component of velocity, w, is located on the filter but the radial component of velocity,

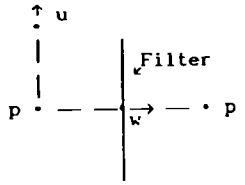

Figure 3. Staggered grid arrangement on filter for velocity components u and w and pressure p.

u, is not located on the filter, being a distance of half a control volume from the filter (see Figure 3). Therefore the modified Darcy law (1) is applied only on the w-component of velocity. For the u-component of velocity, which is in the direction parallel to the surface of the filter, we treat the filter as a porous wall, namely the shear stress on the surface of the filter is determined by the turbulent wall function method.

We now consider an arbitrary volume of fluid which is contained in a volume Ω with an outer surface S and the unit outward normal to the surface is $\mathbf{n}$. We apply the Gauss theorem to equations (2) and (3), which yields their integral forms, i.e.

$$\iint_S \mathbf{V} \cdot \mathbf{n} \mathrm{d}S = 0, \tag{19}$$

$$\iint_S (\mathbf{V} \cdot \mathbf{n}) \mathbf{V} \mathrm{d}S = -\iint_S \mathbf{n} p \mathrm{d}S + \iint_S \mathbf{n} \cdot (\nu_t \nabla \mathbf{V}) \mathrm{d}S - \frac{1}{\rho}(\alpha + \beta|\mathbf{V}|)\mathbf{V}\Omega. \tag{20}$$

The finite difference equations for the velocity components are obtained by using equation (20) for every control volume in the computational domain and introducing an under relaxation parameter E into the momentum equations. In the axial direction this may be expressed in the form

$$a_e\left(1 + \frac{1}{E}\right) w_e = \sum a_{nb} w_{nb} + (p_p - p_E) A_e + \frac{a_e}{E} w_e^o, \tag{21}$$

while in the radial direction we have

$$a_n\left(1 + \frac{1}{E}\right) u_n = \sum_{nb} u_{nb} + (p_p - p_N) A_n + \frac{a_n}{E} u_n^o, \tag{22}$$

where

$$a_n = \sum a_{nb} + \nu_t \left(\frac{\Delta r \Delta z}{r}\right)_n, \tag{23}$$

$$a_e = \sum a_{nb} + \frac{1}{\rho}(\alpha + \beta|\mathbf{V}|)\Omega_e. \tag{24}$$

Here w_{nb} are the values of the w- and u-components of velocity at the nearest-neighbouring points, a_{nb} are the standard maaatrix coefficients, obtained by using the upwind difference scheme, and the coefficients A are the areas of the faces of the control volume.

In the SIMPLEC algorithm the pressure correction can then be obtained by substituting all the velocity components into the continuity equation for the control volume. This yields

$$a_P p'_P = a_E p'_E + a_W p'_W + a_N p'_N + a_S p'_S + b, \tag{25}$$

where

$$a_P = a_E + a_W + a_N + a_S, \qquad a_E = A_e d_e, \qquad a_W = A_w d_w, \qquad a_N = A_n d_n, \qquad a_S = A_s d_s \quad (26)$$

and

$$d_e = \frac{A_e}{a_e - \sum a_{nb}}, \qquad d_w = \frac{A_w}{a_w - \sum a_{nb}}, \qquad d_n = \frac{A_n}{a_n - \sum a_{nb}}, \qquad d_s = \frac{A_s}{a_s - \sum a_{nb}}. \quad (27)$$

The mass residual of every control volume is given by

$$R^k_{\text{mass}} = C_e - C_w + C_n - C_s, \quad (28)$$

where C_e, C_w, C_n and C_s are the masses of fluid convected through each of the faces of the control volume which surrounds the point where the pressure is located. Then the source term in equation (25) is given by

$$b = -R^k_{\text{mass}}. \quad (29)$$

A measure of the rate of convergence of the iterative procedure is the sum of the mass residuals over all the control volumes, namely

$$R_{\text{mass}} = \sum_k |R^k_{\text{mass}}|/(U_0 \pi R^2). \quad (30)$$

5. THE AVERAGE PRESSURE CORRECTION ON THE FILTER

In expressions (23), (24), (26) and (27) we observe that the permeability coefficients α and β are only involved in the axial component of the momentum equations and not in the radial component. For most practical filters the experimental data are usually only sufficient to determine the value of α and therefore in most of this paper we set $\beta = 0$. When one of the permeability coefficients, namely α, of the filter is very large, the pressure drop across the filter is very large. In the example of the 25 mm Millipore membrane filter of type RA, which has a 1·2 μm nominal pore size and a thickness of filter of $L = 1{\cdot}5 \times 10^{-4}$ m, then $\alpha = 2{\cdot}43 \times 10^8$ (and $\beta = 0$) and the pressure drop across the filter is 36,450 N m^{-2} when the velocity is 1·0 m s^{-1}. In such circumstances the pressure drop across the filter is much larger than the pressure variations elsewhere in the solution domain by several orders of magnitude. Although across the filter the pressure change is very large, the coefficients α and β are only involved in the w-component of the momentum equation and in the coefficient a_E of the pressure correction equation when the filter is on the east surface of the control volume for the pressure, or in the coefficient a_w when the filter is on the west surface of the control volume for the pressure. Therefore the pressure equation (25) can inherently produce a sharp change in the pressure on the filter; for example, convergent solutions can be obtained for values of α up to about 10^7 when $\beta = 0$. However, on further increasing the value of α, difficulties arise in obtaining convergent results. In fact, no matter what relaxation factors were used, we could not obtain convergent results when α was larger than about $2{\cdot}0 \times 10^7$. The reason for this is that only the axial momentum equation includes the resistance of the filter, αV. Therefore in the pressure correction equation only the coefficient which is related to the axial component of velocity gives rise to a large pressure correction, but this coefficient is $O(\alpha^{-1})$. However, the coefficient which is related to the radial component of velocity is $O(1)$. Therefore, when α is very large, the coefficient which relates to the pressure correction in the axial direction is very small in comparison with the coefficient which is related to the pressure correction in the radial direction. Then the terms in equation (25) which include the pressure correction in the axial

direction are extremely small and this leads to difficulties in building up the pressure drop across the filter. In order to obtain convergent results for large values of α (and β) and in order to accelerate the rate of convergence for any value of α and β, a new acceleration technique has been developed. In this paper we employ a similar principle to that proposed by Wen and Ingham[1] in order to obtain the average pressure correction on the filter.

On the filter the momentum change in the z-direction and the shear stress caused by the fluid viscosity are both small compared with the resistance of the filter. Thus the Navier–Stokes equation (2) can be simplified to equation (1) and the pressure drop is dominated by the changes that occur in the z-direction. Therefore equation (1) can be approximated by

$$\frac{d\bar{P}}{dz} = -\alpha W - \beta |W| W, \tag{31}$$

where W is the average velocity in the z-direction on the filter and $\bar{P}$ is the average pressure on the filter. If we let W^* be the updated average velocity in the z-direction and W' be the average velocity correction, then

$$W = W^* + W'. \tag{32}$$

By using the global mass conservation principle, we obtain

$$W' = \left(Q - \int_A \rho W^*\right) dS \Big/ \int_A \rho dS, \tag{33}$$

where A is the area of the surface of the filter.

If we let $\bar{P}'$ be the average pressure correction, then the correct average pressure is given by

$$\bar{P} = \bar{P}^* + \bar{P}', \tag{34}$$

where $\bar{P}^*$ is the updated value of the average pressure. Inserting the values of W and $\bar{P}$ from expressions (32) and (34) into equation (31) yields

$$\frac{d\bar{P}^*}{dz} + \frac{d\bar{P}'}{dz} = -\alpha W^* - \alpha W' - \beta |W^* + W'| (W^* + W'). \tag{35}$$

The updated values of velocity, W^* and pressure, $\bar{P}^*$, satisfy equation (31) and W' in the term $|W^* + W'|$ is ignored in order to linearize the equation. Then combining equations (31) and (35) leads to

$$\frac{d\bar{P}'}{dz} = -\alpha W' - \beta |W^*| W'. \tag{36}$$

When the pressure nodes are located on the two sides of the filter (see Figure 3), expression (35) can be modified to the form

$$\Delta \bar{P}' = -(\alpha W' + \beta |W^*| W') \Delta z, \tag{37}$$

where $\Delta \bar{P}'$ is the difference between the pressure corrections on the two sides of the filter and Δz is the mesh size in the axial direction used in the control volume method. Further, we let the average pressure correction in front of the filter take the value of zero and then we obtain the average pressure correction behind the filter as

$$\bar{P}' = -(\alpha W' + \beta |W^*| W') \Delta z. \tag{38}$$

This value for the average pressure correction should then be added to the pressure in the domain downstream of the filter and the pressure in this region then undergoes relaxation, namely

$$P = P^* + \alpha_p \bar{P}'. \tag{39}$$

The relaxation factor α_p should take a small value in order to avoid an overcorrection when α or β is very large; for example, when the value of $\alpha\Delta z = 10^4$ and $\beta = 0$, we set $\alpha_p = 0{\cdot}01$.

The resulting finite difference forms of the momentum equation, the pressure correction equation and the k- and ε-equations are solved using a line-by-line tridiagonal matrix algorithm with one sweep of the momentum equation and four sweeps of the pressure correction equation. The relaxation factor was taken to have a value of $E = 3$ and this produces a stable and convergent result with the fast rate of convergence for all the calculations presented in this paper.

6. RESULTS AND DISCUSSION

For a Millipore membrane filter as used in the experimental investigations of Chung and Ogden[6] the pressure drop across the filter was determined by the modified Hagen–Poiseuille law[7] which has the same form as equation (1), but the permeability coefficient is determined by

$$\alpha = \frac{8\mu}{\pi a^4 N_p (1 + 3{\cdot}992 K_n)}, \tag{40}$$

$$\beta = 0{\cdot}0, \tag{41}$$

where μ is the dynamic viscosity of air.

Although the filter used in the experimental investigation is a 25 mm Millipore membrane filter (type RA, 1·2 μm nominal pore size, $\alpha = 2{\cdot}4 \times 10^8$, $\beta = 0$), we will adopt various values of α in order to investigate the effect of the resistance of the filter on the fluid flow and the convergence behaviour of the numerical methods. Numerical results have been obtained for a wide variety of samplers, but all the results presented in this paper correspond to the experimental data of Vincent *et al.*[5] and Chung and Ogden[6] where $R = 20$ mm, $r_0 = 2$ mm, $r_1 = 11{\cdot}31$ mm, $l = 13{\cdot}2$ mm, $U_0 = 2$ m s^{-1}, $Q = 9{\cdot}6$ l min^{-1} and the average axial velocity at the orifice of the sampler is 12·6 m s^{-1}.

6.1 The enhancement in the rate of convergence for paper filters with a large resistance

The use of the SIMPLEC algorithm and the average line pressure correction formula (37) can produce convergent results very rapidly when the penetration coefficient α is less than about 10^7. However, on further increasing the value of α, a very noticeable reduction in the rate of convergence is obtained. Figure 4 shows the rate of convergence of the mass residual as a function of the number of

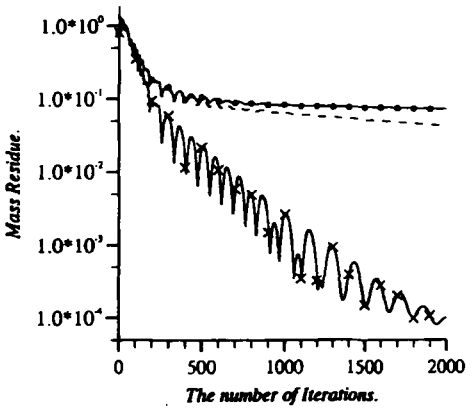

Figure 4. Mass residue as a function of number of iterations: – – –, $\alpha = 3{\cdot}0 \times 10^7$, SIMPLEC; – × –, $\alpha = 3{\cdot}0 \times 10^7$, SIMPLEC with average pressure correction; – o –, $\alpha = 1{\cdot}0 \times 10^8$, SIMPLEC; ——, $\alpha = 1{\cdot}0 \times 10^8$, SIMPLEC with average pressure correction

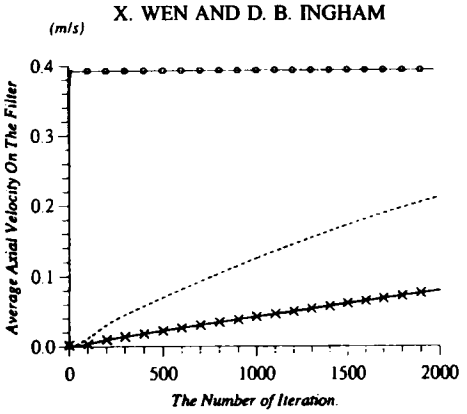

Figure 5. Average velocity on the filter as a function of number of iterations: – – –, $\alpha = 3{\cdot}0 \times 10^7$, SIMPLEC; – × –, $\alpha = 3{\cdot}0 \times 10^7$, SIMPLEC with average pressure correction; – o –, $\alpha = 1{\cdot}0 \times 10^8$, SIMPLEC; ----, $\alpha = 1{\cdot}0 \times 10^8$, SIMPLEC with average pressure correction

iterations for values of $\alpha = 3{\cdot}.0 \times 10^7$ and $1{\cdot}0 \times 10^8$ when using the modified SIMPLEC algorithm as described by Wen and Ingham[1] for speeding up the rate of convergence for fluid flows through a small orifice. It is observed that the mass residual rapidly reduces to a value of about 0·15 during the first 300 iterations for both $\alpha = 3{\cdot}0 \times 10^7$ and $1{\cdot}0 \times 10^8$. However, after this number of iterations the rate of convergence begins to slow down rapidly. After 2000 iterations the mass residuals are 0·0443 for $\alpha = 3{\cdot}0 \times 10^7$ and 0·0725 for $\alpha = 1{\cdot}0 \times 10^8$. We also observe that the larger the value of α, the slower is the rate of convergence of the iterative scheme. Further, we cannot expect that the mass residuals will satisfy the convergence criterion within a reasonable number of iterations. When using the average pressure correction formula (37) to correct the pressure drop across the filter, we observe that the mass residuals for $\alpha = 3{\cdot}0 \times 10^7$ and $1{\cdot}0 \times 10^8$ continue to decrease rapidly as the number of iterations increases and the convergence histories are almost independent of the value of α. Figure 4 shows that after about 2000 iterations the mass residuals have reached a value of about $1{\cdot}0 \times 10^{-4}$. Thus we conclude that the rate of convergence has been significantly improved by adopting the average pressure correction formula (37), because the method quickly produces the rapid pressure drop across the paper filter.

Figure 5 shows the average velocity on the filter as a function of the number of iterations for the same variables and operating conditions as those considered in Figure 4. It is observed that without the use of the average pressure correction formula (37) a very slow rate of convergence is achieved for both the average velocity on the filter and the global mass conservation. Without the use of formula (37), in the case when $\alpha = 3{\cdot}0 \times 10^7$, after about 2000 iterations the average velocity reaches a value of about 0·21 m s^{-1}, while in the case when $\alpha = 1{\cdot}0 \times 10^8$ the average velocity only reaches a value of 0·082 m s^{-1}. It is clear that in order to achieve its correct value of 0·3924 m s^{-1}, an excessively large number of iterations will be required. However, when using the average pressure correction, only 15 iterations are required for the average velocity on the filter to achieve its correct value within an accurcy of 10^{-4}. The average pressure correction formula (37) rapidly builds up the pressure drop on the filter and the global mass conservation is satisfied extremely rapidly.

The streamlines in the vicinity of the sampler for $\alpha = 3{\cdot}0 \times 10^7$ are presented in Figure 6 after 2000 iterations using the modified SIMPLEC technique as described by Wen and Ingham[1] (Figure 6(a)) and with the use of the average pressure correction formula (37) (Figure 6(b)). It is found that the formula for the average pressure correction as proposed by Wen and Ingham[1] rapidly produces the pressure drop at the orifice of the sampler as well as the flux entering the chamber of the sampler, but the velocity field in the vicinity of the filter is very inaccurate. However, when using the average pressure correction formula (37) on the filter, accurate flows may be obtained after about 2000 iterations.

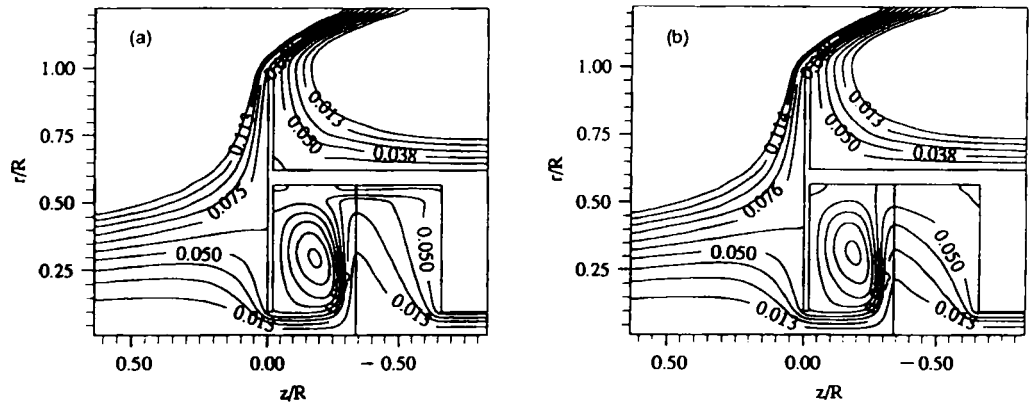

Figure 6. (a) Streamline pattern for $r_1/R = 0{\cdot}567$, $l/R = 0{\cdot}64$, $d/R = 0{\cdot}02$ and $\alpha = 3{\cdot}0 \times 10^7$ when using SIMPLEC algorithm after 2000 iterations. (b) Streamline pattern for $r_1/R = 0{\cdot}567$, $l/R = 0{\cdot}64$, $d/R = 0{\cdot}02$ and $\alpha = 3{\cdot}0 \times 10^7$ when using modified SIMPLEC algorithm[1] and average pressure correction formula (37) after 2000 iterations

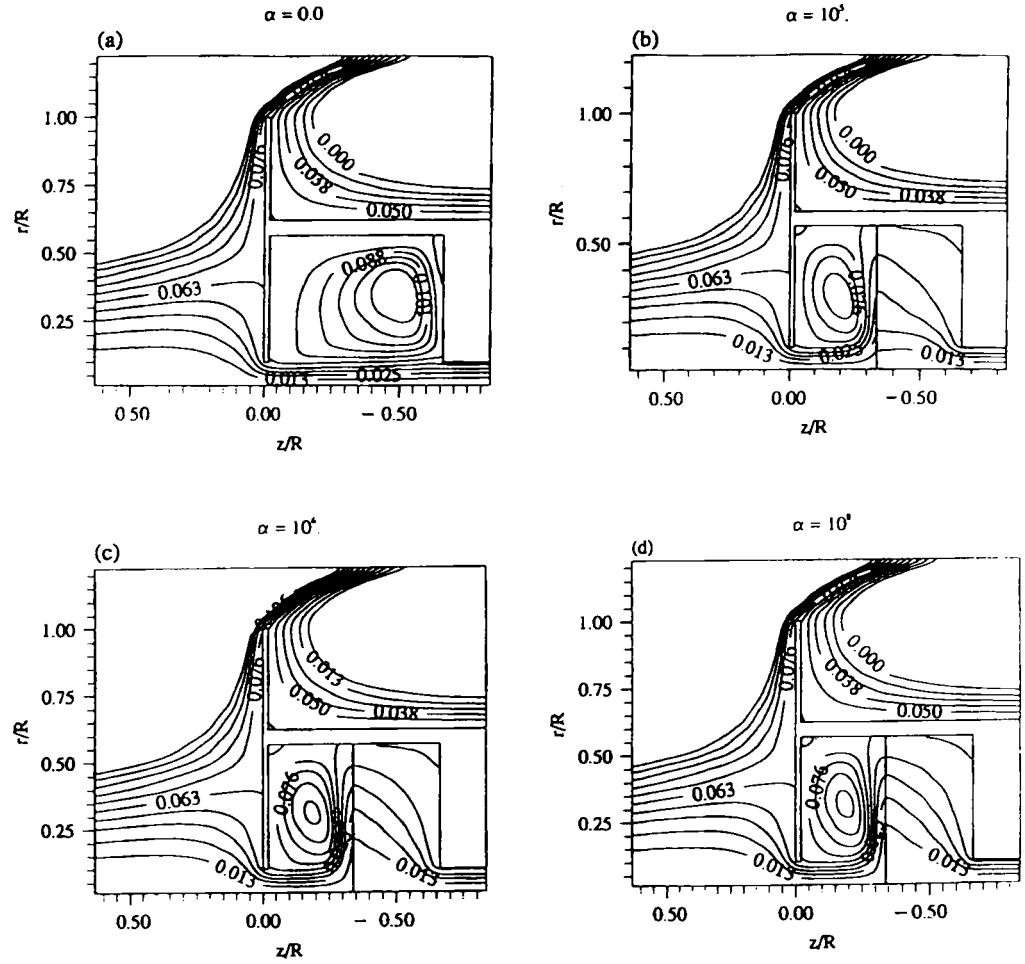

Figure 7. Effect of the filter resistance on fluid flow in sampler for $r_1/R = 0{\cdot}567$, $l/R = 0{\cdot}64$, $d/R = 0{\cdot}02$ (a) $\alpha = 0$, (b) $\alpha = 10^5$, (c) $\alpha = 10^6$ and (d) $\alpha = 10^8$

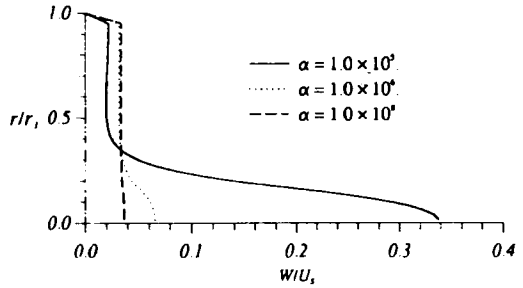

Figure 8. Effect of filter resistance on the axial component of fluid velocity on the filter

The situation where β is in the range $0 \leq \beta \leq 10^8$ has also been investigated for $0 \leq \alpha \leq 10^8$. It has been found that when using the average pressure correction formula (37), the rates of convergence for both the mass residual and the average velocity across the filter are very similar to those in Figures 4 and 5 where $\beta = 0$ and the formula (37) has been used. Thus we conclude that the average pressure correction leads to a rate of convergence which is independent of the choice of values of the coefficients α and β.

6.2. *The effects of the filter on the fluid flow*

When the filter is located at the midplane of the chamber, i.e. 6·8 mm away from the orifice of the sampler, the effect of varying the value of the permeability coefficient of the filter on the streamline pattern is as shown in Figure 7. The solid straight vertical lines within the cylindrical sampler indicate the location of the filter, and the case of $\alpha = \beta = 0$, i.e. no filter, is also presented. We observe that when $\alpha = 10^5$ and $\beta = 0$ the filter produces a very strong resistance to the passage of fluid through it. Two different streamline patterns appear on the two sides of the filter. After passing through the orifice of the sampler, the fluid retains its characteristics owing to its large inertia, but when it reaches the vicinity of the filter, a large quantity of fluid deviates sharply in direction and flows along the plane of the filter before passing through it. As a result of this phenomenon, a strong recirculating flow develops between the front face of the cylindrical sampler and the filter. After the fluid passes through the filter, it is simply sucked into the exit pipe. As the value of α increases, the fluid flow pattern does

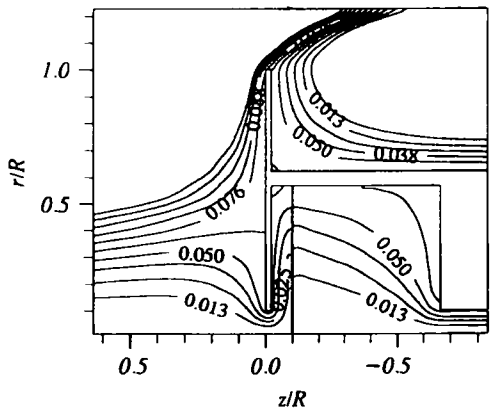

Figure 9. Streamline pattern when the filter is situated very close to the orifice of the sampler for $r_1/R = 0{\cdot}567$, $l/R = 0{\cdot}64$, and $d/R = 0{\cdot}02$.

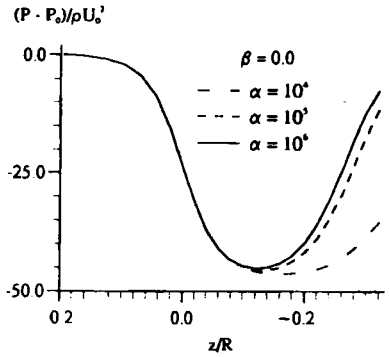

Figure 10. Variation in the pressure on the axis of the sampler between the orifice of the sampler and the filter for $\alpha = 10^4$, 10^5 and 10^6 and $\beta = 0$

not change significantly, but the fluid in front of the filter turns away from the symmetrical axis of the sampler more abruptly. However, after α reaches a value of $O(10^8)$, any further increase in its value only leads to an increase in the pressure drop across the filter and the general fluid flow pattern remains relatively unchanged.

Figure 8 shows the profiles of the non-dimensional axial component of velocity on the filter for various values of α. When there is no filter, the velocity is very large near the axis of symmetry of the sampler, whilst near the wall of the chamber of the sampler the velocity is very small. As the value of the resistance of the filter increases, the magnitude of the axial component of velocity near the axis of symmetry of the sampler decreases, whilst near the wall of the chamber of the sampler the axial velocity increases. Finally, when the value of α is greater than about 10^8, the axial component of velocity at the filter becomes almost uniform and no substantial changes occur as the value of α increases further

When the filter is placed very close to the orifice of the sampler, the resistance of the filter affects the fluid flow pattern near this orifice. Figure 9 shows the streamlines when a 25 mm Millipore membrane filter with $\alpha = 1{\cdot}0 \times 10^8$ and $\beta = 0$ is located at a distance of 2 mm, i.e. one radius of the orifice, from the front face of the sampler. Because the filter is very close to the orifice and the value of α is large, a large fraction of the fluid flow will immediately on entry into the chamber of the sampler turn to flow in the radial direction and no recirculating flow is present in front of the filter. Further, the axial component of velocity through the filter is again almost uniform owing to the large resistance of the filter.

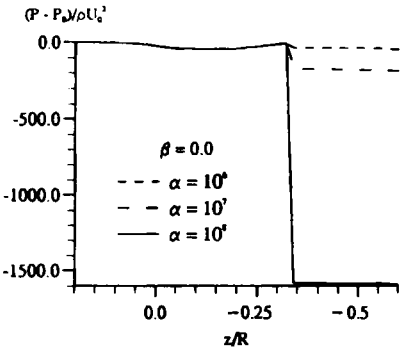

Figure 11. Variation in the pressure on the axis of the sampler between the orifice of sampler and the entrance of the exit pipe for $\alpha = 10^6$ and 10^8 and $\beta = 0$

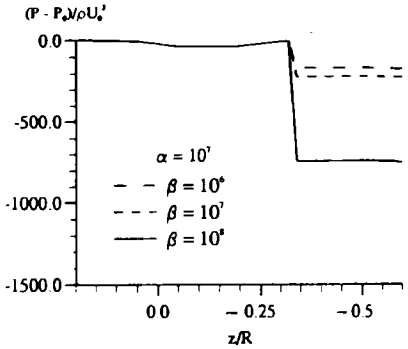

Figure 12. Variation in the pressure on the axis of the sampler between the orifice of the sampler and the entrance of the exit pipe for $\beta = 10^6$, 10^7 and 10^8 and $\alpha = 10^7$

Figure 10 shows the pressure distribution on the axis of the sampler between the orifice of the sampler and the filter for $\alpha = 10^4$, 10^5 and 10^6 and $\beta = 0$. These results show that as the fluid passes through the orifice of the sampler, a large pressure drop in the vicinity of this orifice is always accompanied by an acceleration of the fluid, despite the presence of the filter. However, in front of the filter the pressure undergoes a recovery owing to the resistance of the filter. The pressure increases as the resistance of the filter increases. However, when α is larger than about 10^6, further increase in the resistance of the filter does not cause any increase in the pressure in front of the filter and for a given sampling velocity the upstream pressure distribution of the filter remains almost unchanged.

Figure 11 illustrates the pressure distribution on the axis of the sampler between the orifice and the entrance of the exit pipe of the sampler for $\alpha = 10^6$, 10^7 and 10^8 and $\beta = 0$. It is observed that the resistance of the filter significantly affects the pressure drop across the filter when $\alpha > 10^4$ and that the pressure drop in the vicinity of the orifice of the sampler is much smaller than that across the filter when the resistance of the filter is sufficiently large. Also, although the velocity distribution is only slightly affected by taking the value of α greater than about $2{\cdot}0 \times 10^7$, the pressure drop across the filter still increases as the value of α increases. The effect of the value of β on the pressure drop across the filter has also been investigated and Figure 12 shows the cases with $\beta = 10^6$, 10^7 and 10^8 and $\alpha = 10^7$. It is observed that the effects of the coefficient β on the velocity distribution and the pressure drop are very similar to those of the coefficient α.

7. CONCLUSIONS

The standard k–ε turbulence model has been used for the simulation of turbulent flows both inside and outside a sampler and the staggered grid technique is appropriate for the modelling of the paper filter. In practice paper filters usually have a very large resistance and hence the pressure drop across the filter is very large. When using the SIMPLEC method, it has been found to be very difficult to obtain convergent results. Hence an average pressure correction method has been developed and this has successfully led to a substantial enhancement in the rate of convergence of the iterative scheme. It has been clearly demonstrated that the average pressure correction technique developed in this paper, which is based on the global mass conservation developed by Wen and Ingham,[1] can rapidly build up the average pressure distribution in one direction. This assists the SIMPLE-like algorithms to reveal the local variations in velocity and pressure and to accelerate the rate of convergence of the iterative scheme. The numerical results indicate that the paper filter, which is housed in the sampler, can significantly affect the fluid flow pattern in the chamber of the sampler. Therefore the control of the fluid flow in the chamber can be achieved by appropriately designing the geometry of the chamber. We

have also found that the paper filter as used by Chung and Ogden,[6] produces an almost uniform axial velocity distribution on the filter and this leads to the important conclusion that the velocity profile on this filter is virtually independent of the operating conditions of the sampler if the value of the permeability is larger than about 10^8. This is useful for stable operation of the filter, but if a large pressure drop occurs across the filter, then a more powerful pump is required.

ACKNOWLEDGEMENT

The financial support of the Health and Safety Executive is gratefully acknowledged.

APPENDIX: NOMENCLATURE

d	thickness of disc of sampler
I	turbulent intensity
k	turbulent kinetic energy
L	turbulent length scale
p'	pressure correction
P	pressure of fluid flow
$\bar{P}$	average pressure
$\bar{P}'$	average pressure correction
Q	flux of fluid across filter
r, z	cylindrical co-ordinates
r_1	radius of chamber of sampler
r_2	radius of exit pipe of sampler
R	radius of disc of sampler
R_{mass}	mass residual
U_d	velocity at entrance of exit pipe of sampler
U_0	velocity of freestream
$\mathbf{V}$	velocity vector of fluid flow
W	average axial velocity across filter
y^+	friction length
α, β	permeability coefficients of paper filter
α_p	relaxation factor
ε	turbulent energy dissipation
υ_e	effective viscosity of turbulent fluid flow
υ_t	turbulent viscosity of fluid
υ	viscosity of fluid
ρ	density of fluid
τ_w	shear stress on wall

REFERENCES

1. X. Wen and D. B. Ingham, 'A new method for accelerating the rate of convergence of the SIMPLE-like algorithm'. *Int. j. num. methods fluids*, **15**, 385–400 (1993).
2. S. V. Patankar, *Numerical Heat Transfer and Fluid Flow*, Hemisphere, Washington, DC, 1980.
3. J. P. Van Doormaal and G. D. Raithby, 'Enhancements of the SIMPLE method for predicting incompressible fluid flows', *Numer. Heat Transfer*, **7**, 147–163 (1984).
4. B. E. Launder and D. B. Spalding, 'The numerical computation of turbulent flows', *Comput. Methods Appl. Eng.*, **3**, 269–289 (1974).
5. J. H. Vincent, P. C. Emmett and D. Mark, 'The effect of turbulence on the entry of airborne particles into a blunt dust sampler', *Aerosol Sci. Technol.*, **4** 17–29 (1985).
6. K. Y. K. Chung and T. L. Ogden 'Some entry efficiencies of dislike samplers facing the wind', *Aersol Sci. Technol.*, **5**, 81–92 (1986).
7. C. Orr, *Filtration*, Parts I and II, Marcel Dekker, New York, 1977.